Conformational polymorphic changes in the crystal structure of the chiral antiparasitic drug praziquantel and interactions with calcium carbonate

Ana Borrego-Sánchez[a,b], Esperanza Carazo[b], Beatrice Albertini[c], Nadia Passerini[c], Beatrice Perissutti[d], Pilar Cerezo[b], César Viseras[a,b], A. Hernández-Laguna[a], Carola Aguzzi[b,*], C. Ignacio Sainz-Díaz[a]

[a] Instituto Andaluz de Ciencias de la Tierra (CSIC-University of Granada), Av. de las Palmeras 4, 18100 Armilla, Granada, Spain
[b] Department of Pharmacy and Pharmaceutical Technology, Faculty of Pharmacy, University of Granada, Campus de Cartuja s/n, 18071 Granada, Spain
[c] Department of Pharmacy and BioTechnology, University of Bologna, Via S. Donato 19/2, 40127 Bologna, Italy
[d] Department of Chemical and Pharmaceutical Sciences, University of Trieste, P.le Europa 1, 34127 Trieste, Italy

ARTICLE INFO

Keywords:
Praziquantel
Calcium carbonate
Solid state characterization
DFT calculations
IR spectroscopy
Molecular modeling

ABSTRACT

Praziquantel is an antiparasitic drug used for decades. Currently, the praziquantel commercial preparation is a racemic mixture, in which only the levo-enantiomer possesses anthelmintic activity. The knowledge of its properties in the solid state and other chemical-physical properties is necessary for improving its efficacy and applications. Drug solid dispersions were prepared with calcium carbonate at 1:5 drug to excipient weight ratio by solvent evaporation method. Then, the modification of the crystal structure of the racemic polymorph of praziquantel in presence of calcium carbonate has been studied by means of several analytical techniques (DSC, TGA, XRD, SEM, FTIR, Raman spectroscopy and chiral liquid chromatography). This study has been completed with atomistic calculations based on empirical interatomic force fields and quantum mechanics methods applied to the crystal structure of praziquantel and of intermolecular interactions. The results evidenced that calcium carbonate provoked a conformational change in the praziquantel molecule yielding the formation of different polymorphs of praziquantel crystal. These alterations were not observed replacing calcium carbonate with colloidal silica as excipient in the solid dispersion.

1. Introduction

Schistosomiasis is a parasitic disease caused by *Schistosoma*. It is widely extended, mainly in 78 developing countries in the tropics and subtropics [1–3], and it affects 210 million people approximately, causing two hundred thousand deaths every year. Moreover, at least 92% of people who need treatment for schistosomiasis live in Africa and, behind of malaria, is the second of the most prevalent diseases that affects African children [4].

The infection is caused by the parasite penetration through the skin of healthy individuals, who are in contact with contaminated water. The Schistosomiasis treatment consists in three drugs (oxamniquine, albendazole and praziquantel), due to the fact that prevention is difficult and there is no vaccine. Praziquantel (PZQ) is the most used drug, considering that it has several advantages: i) being active against every Schistosomas species [5] ii) its administration is orally, iii) it produces few side effects, iv) it has a high efficiency, and v) it has low toxicity. For all of these reasons, World Health Organization considers PZQ to be an essential drug [4]. However, its extensive use might produce drug resistance. Another factor, which contributes to drug resistance, is that the drug is only effective against parasite adult forms [6].

PZQ, (RS)-2-(cyclohexylcarbonyl)-1,2,3,6,7,11b-hexahydro-4H-pyrazin[2,1a]-isoquinolin-4-one) [7,8], is a molecule that contains an oxo group in position 4, which is very important for drug activity (Fig. 1). Moreover, if this group is modified, the activity gets suppressed. Furthermore, PZQ has a chiral center in position 11b, therefore, it has two enantiomers with different properties, where only the R-(-)-enantiomer possesses anthelmintic activity [9,10]. However, commercial preparation is a racemic mixture. The process which is the most widely used to obtain enantiomers is the crystallization [11]. The PZQ enantiomeric system behavior was studied at different temperatures and several enantiomer mixtures of PZQ were obtained [12]. Likewise, thermodynamic and solubility properties of PZQ enantiomers were characterized and compared with those of the commercial racemic product [13]. Enantiomers crystals showed different thermal properties relative to the racemic drug and the results of Differential Scanning Calorimetry

* Corresponding author.
E-mail address: carola@ugr.es (C. Aguzzi).

Accepted 26 September 2018

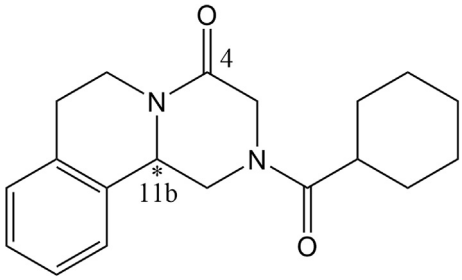

Fig. 1. Molecular structure of PZQ.

(DSC) indicated that the PZQ used is a racemic compound rather than a racemic mixture. Consequently, it is difficult to separate mechanically both enantiomers, unless crystallization and chromatography processes would be used [14]. Moreover, it was possible to combine the racemic PZQ, (RS)-PZQ, with aliphatic dicarboxylic acids to form different co-crystals which differ in their properties, making possible to overcome some of the restrictions on the use of this drug in humans and animals [15]. In addition, PZQ is classified in Class II in Biopharmaceutics Classification System (BCS) [16]. Therefore, the improvement of PZQ dissolution rate and/or solubility has an important technological interest [17]. Solid dispersions prepared by melt granulation and spray congealing showed their efficacy in enhancing the PZQ dissolution rate [18]. Recently, clay minerals as montmorillonite and sepiolite were studied as nanocarrier with the aim of improving the biopharmaceutical profile of the drug [19]. More recently, a new PZQ polymorphic phase, called Form B, has been discovered and fully characterized demonstrating better bioavailability in term of intrinsic dissolution and solubility [20].

Ground calcium carbonate (GCC) is a pharmaceutical excipient widely used as a diluent in solid dosage forms, as an adjuvant in dissolution for dispersible tablets, as a food additive and calcium supplement [21]. GCC is a natural and economic component for pharmaceutical and veterinary drugs with an interesting potential use in developing countries. Therefore, calcium carbonate has been proposed as excipient for a new delivery system of low soluble drugs, e.g. praziquantel. In particular PZQ-GCC solid dispersions were prepared by solvent evaporation method and then characterized to detect possible drug solid state modifications or interactions with the excipient. This is important because the characterization and stability of chiral drugs properties in solid state are critical for their development, manufacturing and applications. Previous solubility studies of PZQ reported ambiguous behavior due particularly to the existence of crystal polymorphism [11,12,14]. Thus, the main aims of this work were to investigate the physico-chemical characteristics of the racemic crystal form of PZQ once in contact with powdered calcium carbonate, by means of DSC, TGA, XRD, SEM, FTIR, Raman spectroscopy and chiral chromatography. Finally, the relationships between the different crystal forms of PZQ at molecular scale were discussed.

2. Experimental section

2.1. Materials

Praziquantel (PZQ) was kindly donated by Fatro S.p.A. (Bologna, Italy). Calcium carbonate, as Ground Calcium Carbonate Calcitec Pure PH V/40S (GCC), was purchased from Italy (Company “Mineraria Sacilese”). The Calcium Carbonate Calcitec Pure PH is used in the food industry and in industries where a low content of heavy metals is requested as well as in the pharmaceutical industry, since it was accepted in the latest edition of the European Pharmacopoeia and the USP. Colloidal silica (Aerosil® 200) was purchased to Degussa AG (Frankfurt). Ethanol of 96% and 99% of purity were used as PZQ solvents.

2.2. Preparation of the PZQ and GCC interaction product (IP)

An amount of GCC was dispersed in an ethanolic solution of PZQ under magnetic stirring at room temperature and protected from light to obtain a drug/calcium carbonate ratio of 1:5 w/w. After 24 h, the solvent was evaporated at 40 °C with a rotary evaporator (Buchi® R II) at reduced pressure. The solid residue was dried in a desiccator and then it was pulverized. The obtained solid dispersions were stored in a desiccator at room temperature. As a control experiment, comercial PZQ was treated without GCC following the same procedure (PZQ_c). Colloidal silica was also used instead of GCC in the same way for comparison purposes.

2.3. Powder X-ray diffraction

Powder X-ray diffraction was performed with a Philips® X-Pert diffractometer with Cu Kα radiation. The information of diffraction was analyzed using XPOWDER® software [22].

2.4. Thermal analysis

Differential Scanning Calorimetric analysis (DSC) and thermogravimetric analysis (TGA) were performed with a Mettler Toledo mod. TGA/DSC1 calorimeter, equipped with sensor, a FRS5 microbalance (precision 0.1 μg) and the FP89 software package. A heating rate of 5 °C/min was used in the 30–400 °C temperature range for TGA and DSC runs. Additionally, a rate of 2 °C/min was used for some specific DSC runs. Nitrogen was used as purge gas in DSC under flows of 15 mL/min^{-1}.

2.5. Scanning electron microscope (SEM)

Microphotographs of the samples were performed using a Hitachi S-510 scanning electron microscope (voltage 25 kV, secondary electron images) (Hitachi Scientific Instruments Ltd, Tokyo, Japan). The samples were mounted on adhesive paper, fixed with colloidal gold and metallized with gold in two orientations (20–30°). The images were captured digitally using the program ScanVision 1.2 attached to the microscope.

2.6. Fourier Transform Infrared (FTIR) and Raman spectroscopies

Fourier Transform Infrared Spectroscopy (FTIR) spectra were recorded in the range 4000–600 cm^{-1} with a 0.5 cm^{-1} resolution and a well-plate sampler (JASCO 6200 spectrophotometer with Spectra Manager II software). Raman spectra were recorded in the range 3500–800 cm^{-1} with a 6.48 cm^{-1} resolution using a Micro-Raman dispersive JASCO NRS-5100 spectrophotometer, with laser light source VIS-NIR, red diode at 785 nm with 500 mW of power (*TorsanaStarbright*), refrigeration by air and a KnowItAll JASCO Edition for Raman software.

2.7. High-performance liquid chromatography (HPLC)

The chirality of drug in the interaction product was measured by high-performance liquid chromatography (HPLC), using a 1260 Infinity II Agilent equipment (G) with quaternary pump, autosampler, column oven and UV-VIS diode-array spectrophotometer. The stationary phase was a column Chiralpak® IC, 5 μm, 150 × 4.6 mm (Daicel Corporation), and the mobile phase was a mixture of H_2O and CH_3CN (35:65 v/v). The flow rate was set at 0.8 mL/min with an injection volume of 10 μL. A detector with a wavelength of 225 nm was used and the run time for each analysis was 5 min. Data were recorded and analyzed by using LC Open LAB HPLC 1260 software (Agilent, G).

3. Computational section

The Compass FF [23] based on empirical interatomic potentials was used within the Discover program of the Materials Studio package on the periodical crystal models [24]. This FF was used previously to describe PZQ molecules and crystal structure with satisfactory results [25]. An atomic interactions cut-off of 18.5 Å was used for calculating Van der Waals and Coulomb interactions.

Additional DFT calculations of the periodic racemic crystal of PZQ were also performed with the SIESTA program [26] using the generalized gradient approximation (GGA) with the Perdew–Burke–Ernzerhof (PBE) [27] correlation exchange functional, and norm-conserving pseudopotentials [28]. Preliminary calculations were set up to explore different values of mesh cut-off energy and different numbers of *k*-points in the irreducible wedge of the Brillouin zone to optimize the calculations level. A wide range of mesh cut-off energy values in steps of 50 Ry was explored according to previous work [29,30], finding a suitable cut-off energy of 800 Ry and two *k*-points in the Brillouin zone in this work.

Powder XRD patterns were simulated from crystal structures by using the Reflex code implemented in Materials Studio package [24].

4. Results

4.1. Physico-chemical evaluation of PZQ-GCC interaction product

Possible interactions between PZQ and GCC were first explored by powder XRD on pristine PZQ, GCC and the IP obtained by solvent evaporation using ethanol 96% (Fig. 2). The pristine PZQ was solved and recrystallized through the same procedure evaporation of ethanol 96%, as a control experiment without GCC, and its XRD pattern showed a crystalline PZQ according with that previously reported [31] (Fig. 2a). GCC shows a typical pattern of calcite with reflections at 23.0°, 29.4° (the most intense), 39.5° and 43.1° (2Θ units).

The IP mixture showed reflections of mainly calcium carbonate crystals. Reflection peaks of PZQ crystals in IP had very low intensity and resolution probably due to the amorphization of PZQ or several changes in the crystallinity of the PZQ crystals with GCC as explained later. In previous works a similar behavior of PZQ was observed in the formation of a solid dispersion with polyvinylpyrrolidone (PVP) [32], sodium starch glycolate [33] and clay minerals [19]. The powder XRD pattern of a physical mixture (PM) of PZQ with GCC showed that the crystallinity of PZQ was maintained corroborating that the treatment of GCC and ethanol 96% affects the crystallinity of PZQ (Fig. 2b).

Thermogravimetric profiles of the samples studied are shown in the Fig. 3. GCC shows a slight weight loss (0.34% w/w) at 40 °C approximately, corresponding to the surface humidity evaporation. PZQ weight loss occurs in the range between 200 and 422 °C (97.64% w/w) due to the decomposition of PZQ. The IP showed similar profiles with the decomposition of the PZQ fraction at 250–300 °C, indicating the PZQ is remained in the IP, although the thermal range is narrower than the pure PZQ. This range can be due to a different crystallinity of PZQ in the IP.

The DSC profiles of these samples are reported in Fig. 4. PZQ showed a strong endothermic peak at 142–144 °C corresponding to the melting of the (RS)-PZQ crystal. GCC showed no significant peak in the DSC profile at T < 200 °C. The IP profile was completely different that pure PZQ and GCC, displaying two small peaks at 110–112 °C and around 133–144 °C. Since no weight loss was observed by TGA at this temperature range, the peak at about 110–112 °C could be attributable to the melting of either the monoenantiomeric crystals or of the new polymorph (Form B) described recently by Zanolla et al. [20], both reported at around 111 °C. The second endothermic peak at higher temperature could be ascribed to possible agglomerate or pseudoracemate crystals (134–138 °C) according to a previous work [11]. Finally, the broad and weak shoulder around 142–143 °C corresponded to the initial racemic (RS)-PZQ crystals. Therefore, the formation of a disordered mixture of several crystal forms in IP could justify the low resolution of the PZQ reflections in the XRD pattern.

In order to obtain better DSC profiles with more accurate melting points and for comparisons with previous studies [14], a lower temperature rate (2 °C/min) and gas flow (15 mL/min) was used confirming the above profiles. An experimental control of pristine PZQ treated was performed with ethanol 96% following the same procedure as the IP. The treated PZQ showed its endothermic peak at 142 °C (Fig. 5a) with a melting enthalpy of $\Delta H = 90.4$ J/g according to previous work [32]. On the contrary, the IP mixture showed endothermic peaks at 112 °C, 134 °C and 138 °C (Fig. 5b). Similar DSC profile was found by De la Torre et al. [32] in IP of PZQ with PVP. The peak at 134 °C disappeared after 3 months from preparation, increasing the area of the peak at 138 °C. This can indicate that the crystal form with the melting point at 134 °C was metastable and transformed slowly to the form which melted at 138 °C. Therefore, we can conclude that the alteration of PZQ solid state within the IP mixture was not due to the dissolution-evaporation process, but it is due the direct interaction of PZQ with GCC.

SEM microphotographs of GCC (Fig. 6A) showed a grain size lower than 10 μm, with typical morphologies of GCC of high purity for pharmaceutical use previously reported [21]. Particles associated with any impurities were not detected, corroborating the XRD results. The micropictures of the racemic (RS)-PZQ (Fig. 6B) presented elongated prismatic morphology and sizes superior to 100 μm, similar to those observed for drug racemic mixture previously [11,15].

In the SEM micropictures of the IP, significant changes of size, texture and morphology were observed (Fig. 6C and D). Filamentous particles interconnecting the GCC particles were observed along with some wider needles. The initial particles of PZQ disappeared and PZQ formed aggregates on the GCC particles during the dispersion and solvent evaporation process and the filaments grew inside these aggregates. This small crystal size of these disordered fibers can justify the low crystallinity and the above lack of XRD reflections in this IP mixture. A similar behavior was observed in previous works when PZQ is mixed with PVP in a solid dispersion [32], with sodium starch glycolate [33], and with clay minerals [19], where the formation of similar fibers was observed after preparation of IP. Recently this formation of fibers of PZQ was also observed after neat grinding without additives, and it was attributed to the new PZQ polymorphic form (Form B) [20], which can be in agreement with the 112° peak of our DSC analysis. However, in our experimental control the PZQ recrystallized in EtOH 96% in the same conditions as IP showed a similar crystal shape and morphology that the pristine PZQ in the SEM micropictures (Fig. 6E and F). This corroborates the effect of water and GCC on the crystallinity of PZQ.

FTIR spectra of the racemic PZQ, calcium carbonate (GCC) and the IP are compared in Fig. 7. PZQ shows two main characteristic bands in the range 2960–2840 cm^{-1} assigned to stretching vibration modes ν(CH) of CH and CH_2 groups [18]. Two bands corresponding to the ν(C═O) vibration mode are observed at 1665–1621 cm^{-1} [18], which can be assigned to each carbonyl group with different local environment in the crystal packing. The δ(C—H) and ν(C—N) modes are observed around 1350–1021 cm^{-1} [34]. The spectrum of GCC shows characteristic bands of the carbonate group (CO_3^{2-}) at 1453, 875 and 712 cm^{-1} [35,36]. In the IP, the bands of PZQ were detected with lower intensity than in the pure product, but most of them overlap with the bands of Ca carbonate due to the high proportion of GCC. However, slight differences can be distinguished in the ν(C═O) bands. In PZQ, two ν(C═O) bands appear with maxima at 1647 and 1624 cm^{-1}, corresponding to the syn relative conformation of the carbonyl groups in the (RS)-PZQ crystal. The shoulders observed at higher frequency are assigned to the syn conformation in twisted planes of each C═O group, according to previous work [37]. On the contrary, in IP these bands are broader with maxima at 1644 and 1634 cm^{-1}. These frequency shifts could also be assigned to the conformation change of the C═O groups in an anti conformer whose frequencies are closer according our

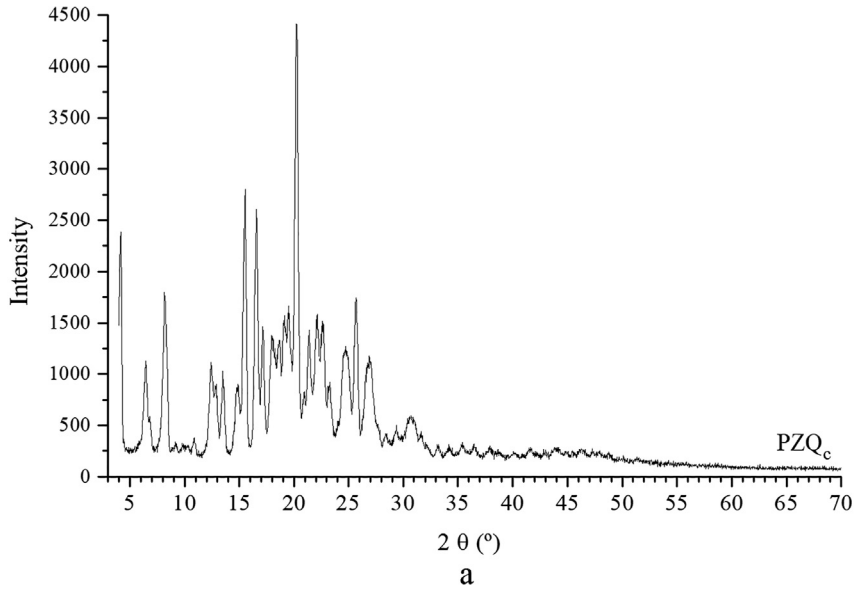

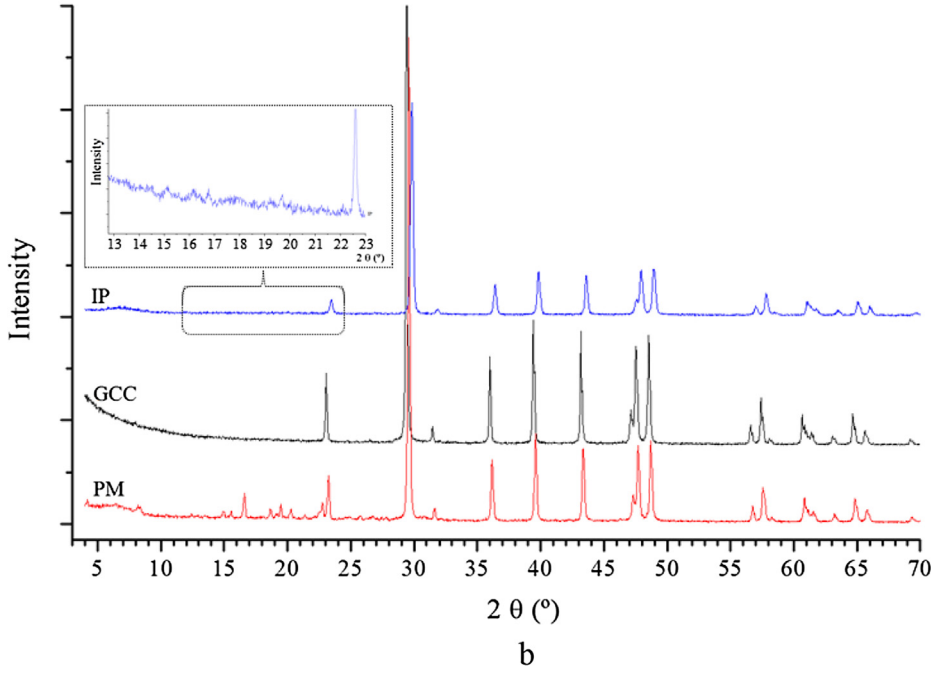

Fig. 2. Powder XRD patterns of the studied samples, PZQ obtained crystalized through ethanol 96% evaporation (a), IP, GCC, and PM samples (b).

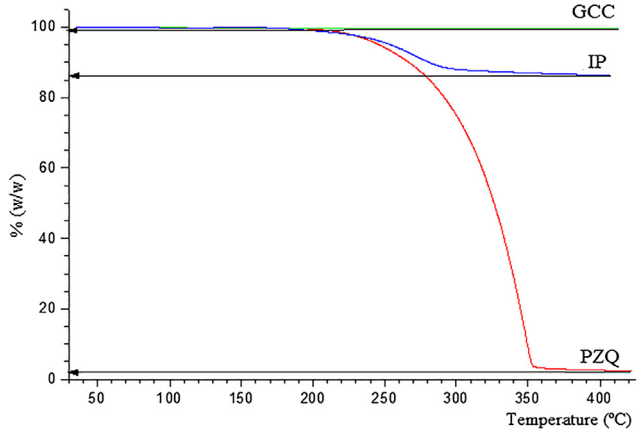

Fig. 3. TGA profiles of the studied samples.

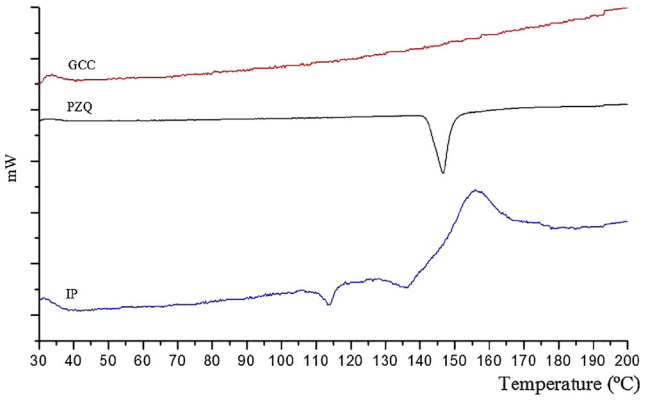

Fig. 4. DSC profiles of GCC, PZQ, and the IP.

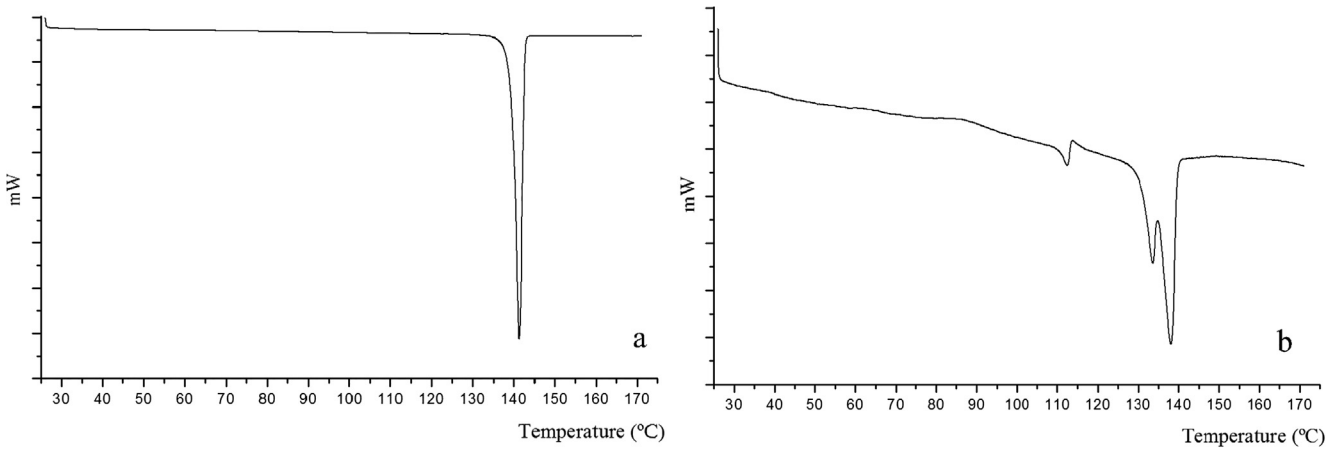

Fig. 5. DSC profiles of PZQ treated with ethanol 96% (PZQ_c) (a), and the IP (b).

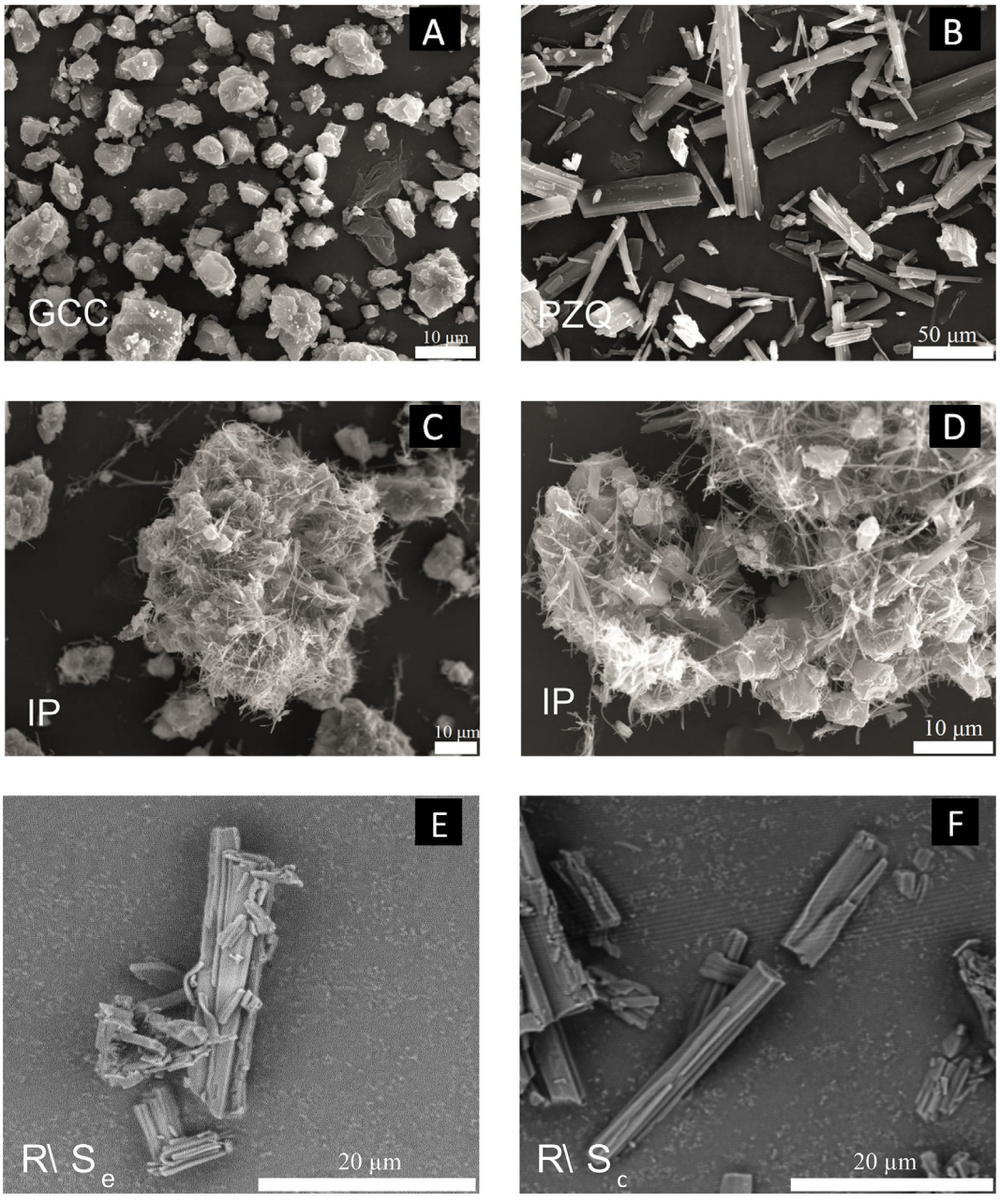

Fig. 6. SEM microphotographs of studied samples at different magnifications.

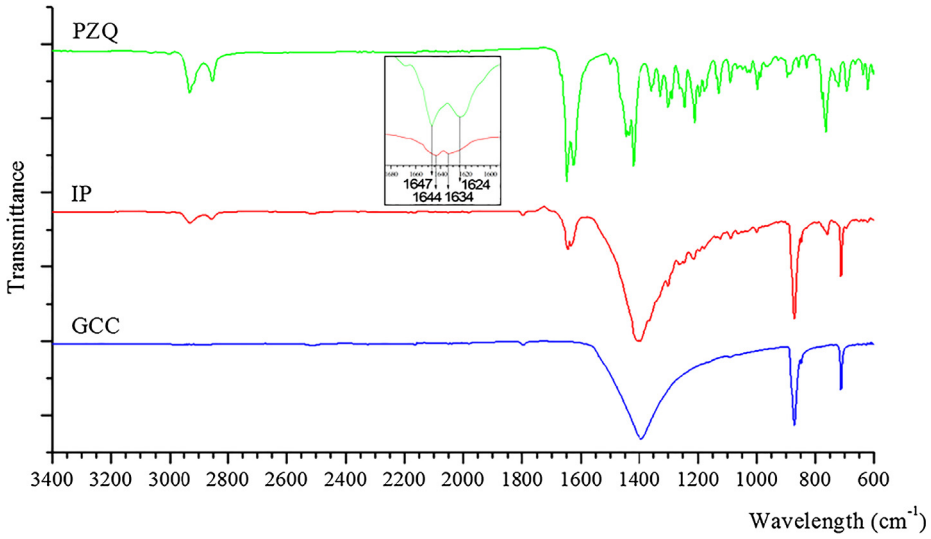

Fig. 7. FTIR spectra of PZQ, the IP, and GCC.

previous calculations [37]. This frequency shifts were also previously observed for the Form B phase [20]. These bands are broader due to the co-existence of several conformations, syn and anti, confirming the mixture of crystal forms detected above.

In addition, the Raman spectra of PZQ (Fig. 8) shows a high intensity band at 1044 cm^{-1} that can be assigned to a symmetric deformation vibration mode of C-N, $\delta(CN)_s$. Whereas the most intense band of the calcium carbonate (GCC) spectra appears at 1085 cm^{-1}, that corresponds to the symmetric ν(C—O) stretching [38–40]. The intensities of the PZQ fraction of the IP mixture are very low indicating the possible formation of different PZQ crystal forms. Nevertheless, the main bands of PZQ can be weakly observed in the IP spectrum. However, slight differences can be detected in the ranges of 1150–1250 cm^{-1}, and 1280–1360 cm^{-1} where the profiles are different and closer to the calculated anti conformer of PZQ [37]. Hence this enforces the existence of other crystal forms with different conformer mixture.

In addition, the chirality of the drug in the IP was measured by high-performance liquid chromatography (HPLC), obtaining the same proportion of each enantiomer in pure PZQ and IP, which means that the IP obtained was still a racemic product (Fig. 9). Taking into account the melting point observed at 111 °C in DSC, we tried to separate this melted phase from the rest of crystal form and observe possible changes in the enantiomer proportion by HPLC. Then, we placed an IP solid sample on a mesh and heated it for 3 h at 125 °C. No melted material was observed with shorter heating time. The melted part was absorbed by an absorbent paper placed below the mesh. Subsequently, this paper was treated with ethanol 96% to extract the melted compound and this dissolution was analyzed by HPLC. The chromatogram showed (Fig. 9c) a greater proportion of the area of peak that appeared at a time of retention of 6 min, approximately. However, this peak appeared as a double peak, suggesting the overlapping of two compounds formed during the heating of the IP at 125 °C. Other peaks with low retention time are observed, indicating other different compounds formed during

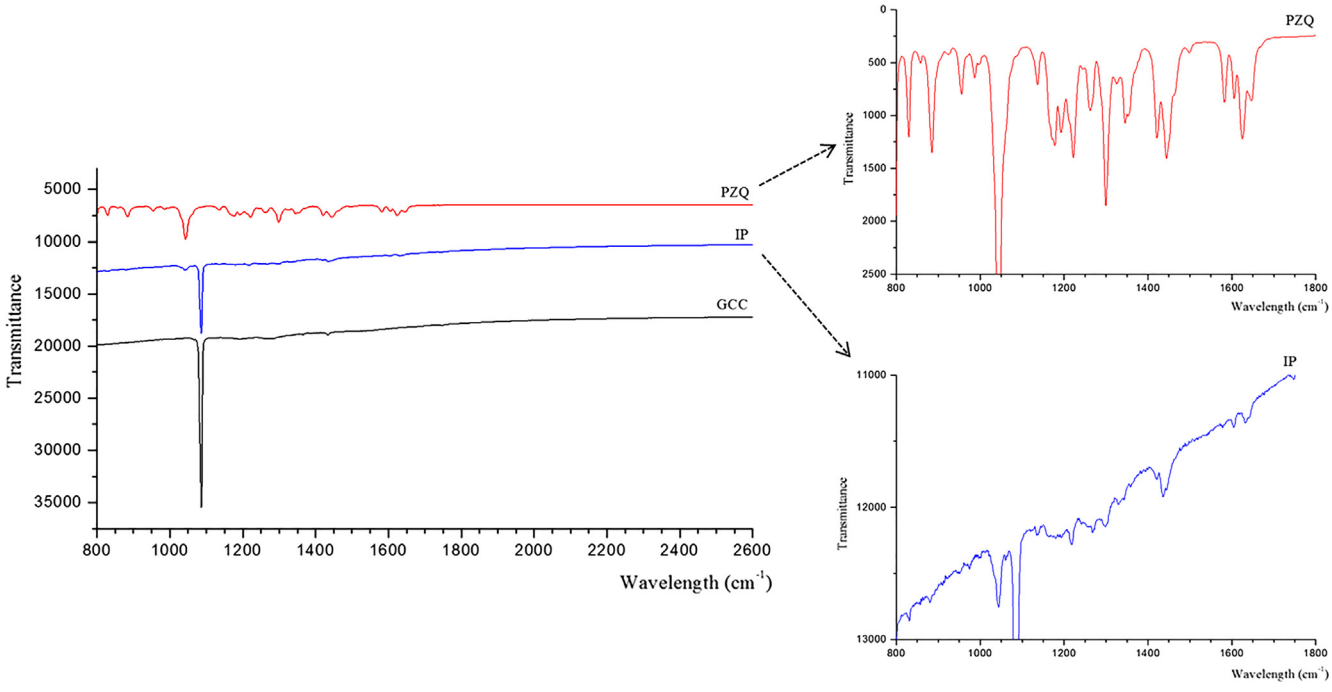

Fig. 8. Raman spectra of PZQ, the IP, and GCC.

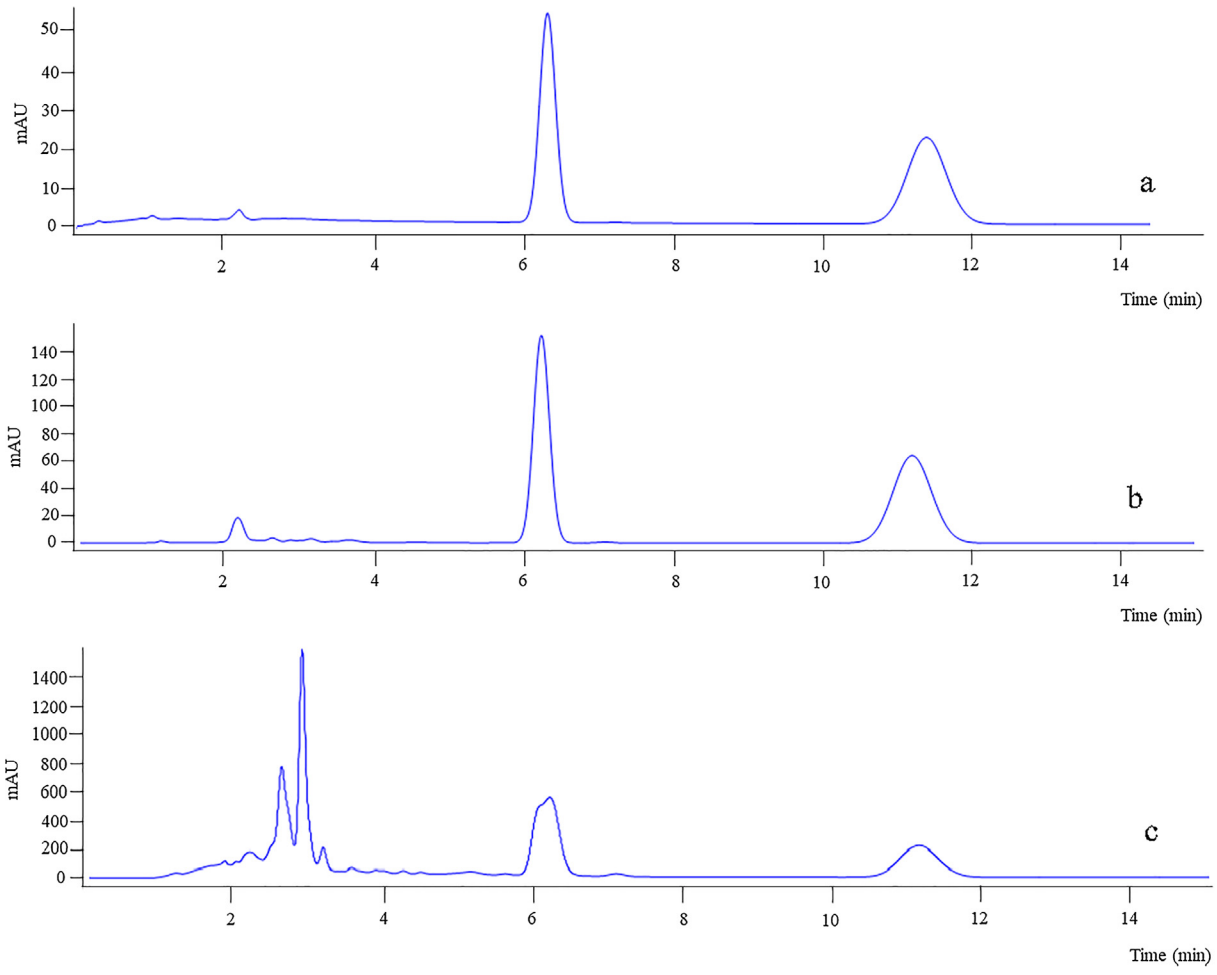

Fig. 9. HPLC chromatograms of the pure PZQ (a), IP (b), and the melted part of the IP after 3 h at 125 °C (c).

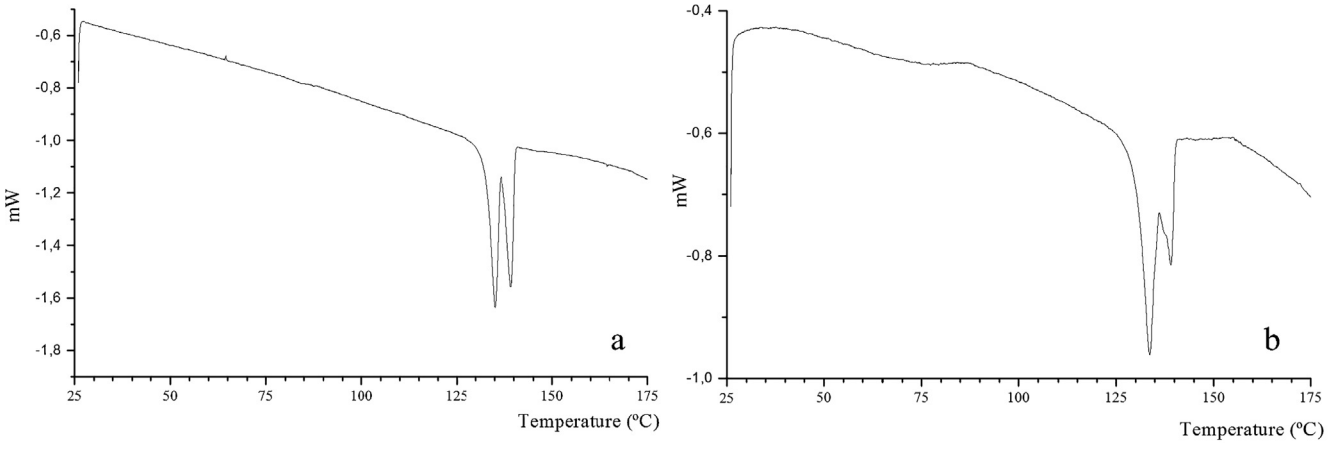

Fig. 10. DSC profiles of PZQ treated with ethanol 99% in GCC during 24 h of agitation (a), in GCC during 72 h of agitation (b).

the heating process.

To confirm this hypothesis, this experiment was repeated by using DSC, treating the IP at 125 °C for 3 h. After that process, the DSC profile was gone on by heating up to 400 °C, then a subsequent cooling process up to room temperature was followed (Fig. S1). An exothermic peak was observed at 110–125 °C corresponding to the decomposition of the compound instead of the melting endothermic peak of Form B crystal phase (Fig. S1a and S1b). The shoulder at 111 °C could indicate a balance between the melting and decomposition of the Form B. This degradation was small maintaining the main molecular structure, because the main degradation occurred at 210–310 °C. In N_2 atmosphere, the degradation decreased, the melting peak of (RS)-PZQ crystal was observed at 134–140 °C and the main thermal degradation occurred at a higher temperature range, 270–350 °C. As a result, the degradation of the drug was observed (Fig. S1). Therefore, the alteration of the HPLC chromatogram of the IP treated at 125 °C was due to the PZQ degradation. By performing the DSC scan of the pristine PZQ sample no degradation of the drug was observed (Fig. S1c). No peak was observed during the cooling process indicating no recrystallization of the initial compound confirming the total degradation of PZQ. Therefore, this

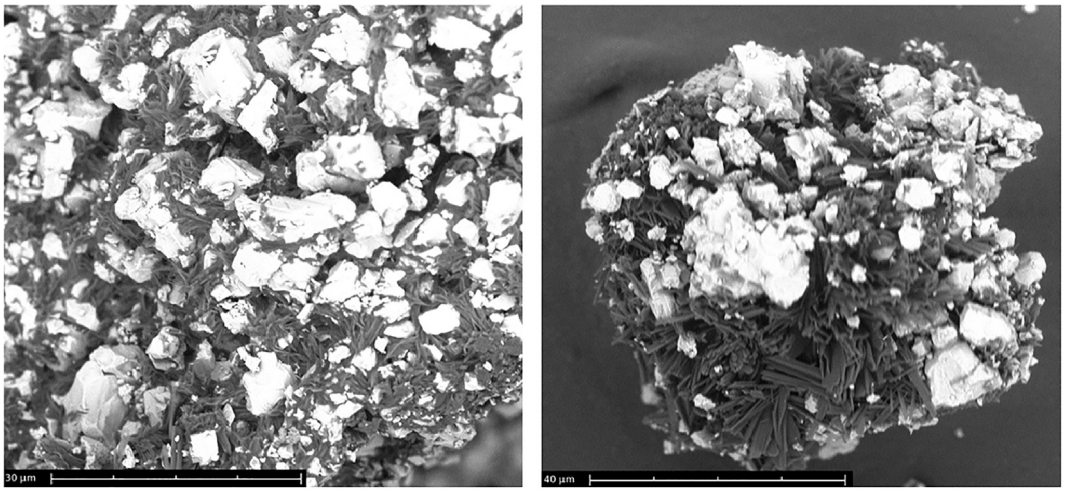

Fig. 11. SEM microphotographs of the PZQ treated with ethanol 99% in GCC during 24 h of agitation and afterwards solvent evaporation.

means that when the IP was maintained at 125 °C for 3 h, the crystal form, which has a melting peak of 112 °C, degrades under these conditions, while the rest of the sample does not degrade until T > 210 °C.

4.2. Interaction products of PZQ in other conditions

Other experimental conditions have been explored, such as the influence of a more pure ethanol to minimize the presence of water and contact time in the formation of IP in the same conditions as in the above experiments. The DSC profile of the PZQ treated with ethanol 99% and GCC showed endothermic peaks only at 134 °C and 138 °C (Fig. 10a). Therefore, the peak at 112 °C only appears with ethanol 96% (with 4% of water). On the other hand, the contact time was also explored considering 24 and 72 h with ethanol 99%. The same behavior was observed. The DSC profile showed endothermic peaks only at 134 °C and 138 °C (Fig. 10b). The peak at 134 °C was more intensive than the other peak, and no peak at 112 °C was found.

In the micropictures (SEM) of PZQ treated with ethanol 99% in GCC for 24 h and afterwards solvent evaporation, the crystal particles were different and smaller than those of pristine PZQ (Fig. 11 and Fig. 6B, respectively). No filamentous fibers, similar to those found in the IP obtained with ethanol 96% (Fig. 6C and 6D), were observed. Therefore, the presence of water resulted fundamental for the formation of the crystal forms with melting point at 112 °C.

The behavior of PZQ in interaction with a less reactive compound like colloidal silica was tested in the same conditions that with GCC. PZQ was treated with colloidal silica in ethanol 99% and ethanol 96% during 24 h of agitation and afterward ethanol evaporation. DSC profiles showed a single melting peak at 140 °C, without splitting of peaks (Fig. 12). The peak is typical of pure PZQ. No formation of the crystal form with melting point at 112 °C was observed. Therefore, the presence of GCC is critical for the change in the crystallinity of PZQ.

5. Discussion

5.1. Interactions between PZQ and calcium carbonate at molecular level

Our experiments described above indicated that the interaction of the (RS)-PZQ solid with calcium carbonate affects the crystallization process and crystallinity of PZQ, forming other different crystal forms. No chemical decomposition of PZQ was observed, but only alterations of the ordering in the packing of PZQ molecules and a conformational change in the PZQ molecule. In the (RS)-PZQ crystal the carbonyl groups are oriented to the same direction, *syn* conformation (Fig. 13a). During the nucleation step, the calcium carbonate can interact with these carbonyl groups of PZQ. This interaction can be enhanced with the presence of a small amount of residual water coming from the ethanol (96%) solvent during the treatment. Previous calculations showed that the *syn* conformation of PZQ is the more polar than the *anti* one [37] (Fig. 13b) and it is likely to be present in an ethanol/water solution during the formation of the solid dispersion. Then, both conformers can be present in the solution and form different crystal nuclei. Our FTIR analysis indicates the presence of several conformers in the broadening of the stretching C═O bands in IP sample (Fig. 7).

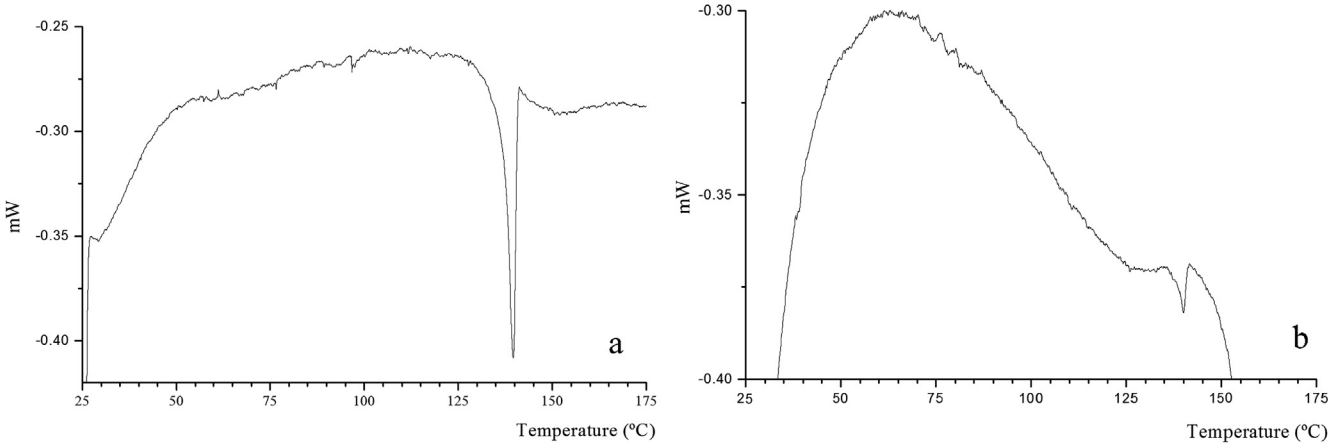

Fig. 12. DSC profiles of PZQ treated in colloidal silica with ethanol 99% (a) and in colloidal silica with ethanol 96% (b).

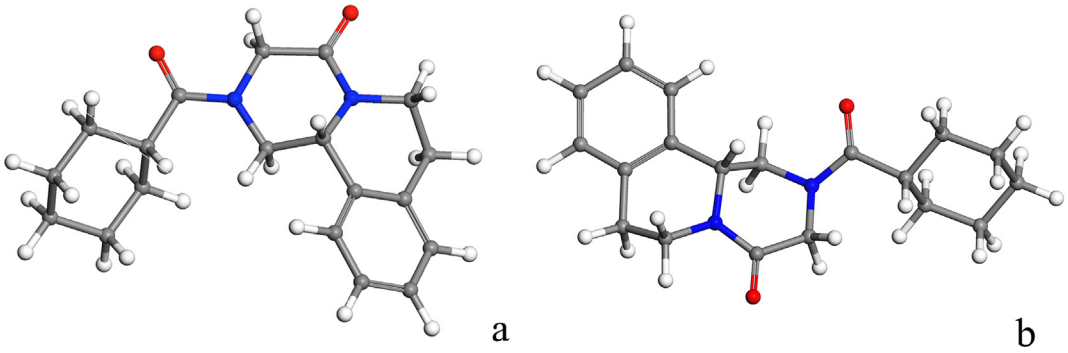

Fig. 13. Conformations *syn* (a) and *anti* (b) of PZQ. The C, H, N, and O atoms are in grey, white, blue, and red color. (For interpretation of the references to color in this figure legend, the reader is referred to the web version of this article.)

Our above experiments indicate that the interaction of PZQ with water and GCC is critical for the crystallinity alteration in the IP samples. The presence of water/carbonate alters definitely the recrystallization of PZQ. Possibly, a local zone of high pH aqueous conditions could affect in this recrystallization during the nucleation and ordering of the PZQ units. However, we cannot measure the pH at nanoscale level. Nevertheless, we include here this idea as a hypothesis and as a starting point for future investigations. Definitely the actual effect will be the interactions at molecular level in a PZQ/water/$CaCO_3$ complex. In order to explore these interactions, we can create small models to describe this complex system with only one PZQ molecule, one water molecule and one GCC salt complex. We understand that these models can be considered too small. But these models do not pretend to reproduce exactly the experimental scenario, that would be too complex and difficult to calculate. Our models represent the minimal expression to describe the formation of interatomic interactions between PZQ/water/$CaCO_3$. Of course this complex will be surrounded by more water molecules and $CaCO_3$ species but they will be in outer coordination spheres.

Then, two possible complexes can be considered: PZQCCw1, where the Ca^{2+} cation is coordinated with both carbonyl groups in a equidistant distance of 2.9 Å; and PZQCCw2, where the water molecule interacts directly with both carbonyl groups by means of hydrogen bonds at 2.3 Å. Both models were generated and the geometry was optimized with Compass FF calculations, using the SPC water model. In both models the coordination changed to only one carbonyl group during the optimization process. In PZQCCw1, the Ca^{2+} cation is coordinated at 2.30 Å to only one carbonyl O atom, which is joined to the cyclohexyl ring, leaving free the other carbonyl group; and the water H atoms form hydrogen bonds with the carbonate O atoms at 1.48–1.52 Å (Fig. 14a). Similarly in PZQCCw2, one water H atom is coordinated at 1.73 Å to only one carbonyl O atom, which is joined to the cyclohexyl ring, leaving also free the other carbonyl group (belonged to the heterocyclic ring), and the water O atom is coordinating the Ca^{2+} cation *d* (O···Ca) = 2.25 Å (Fig. 14b).

In both models the Ca^{2+} cation is coordinated to two carbonate O atoms at 1.87–1.91 Å. It is remarkable that in both complexes the heterocyclic carbonyl moiety is not coordinated being more free for rotating to the *anti* conformation facilitating the formation of other crystal forms as observed experimentally.

5.2. Molecular interactions in the conformational changes of PZQ in the crystal forms

In the above experiments the racemic crystal of (RS)-PZQ was partially decomposed on other crystal forms owing to the interaction with GCC during the nucleation and recrystallization of PZQ. The molecular interactions in the different crystal forms can be explored at molecular level by means of molecular modeling simulations to explain this experimental behavior. In this work, the intermolecular interactions within the different crystal forms are analyzed more exhaustively. The crystal structures of the R enantiomer of PZQ, the commercial racemic (RS)-PZQ and the new polymorph of (RS)-PZQ, form B proposed by Zanolla et al. [20], were calculated at molecular level and compared. All details of these calculations are described in the Supplementary material.

The crystal lattice of (RS)-PZQ is formed by enantiomer pairs and the molecular packing is due to the electrostatic interactions of the carbonyl groups with the H atoms of the heterocycles and π-π interactions between aromatic and heterocyclic rings (Fig. 15a). The difference between the (R)-PZQ and (RS)-PZQ crystals is not only the proportion of enantiomers, but they are different crystal forms, with

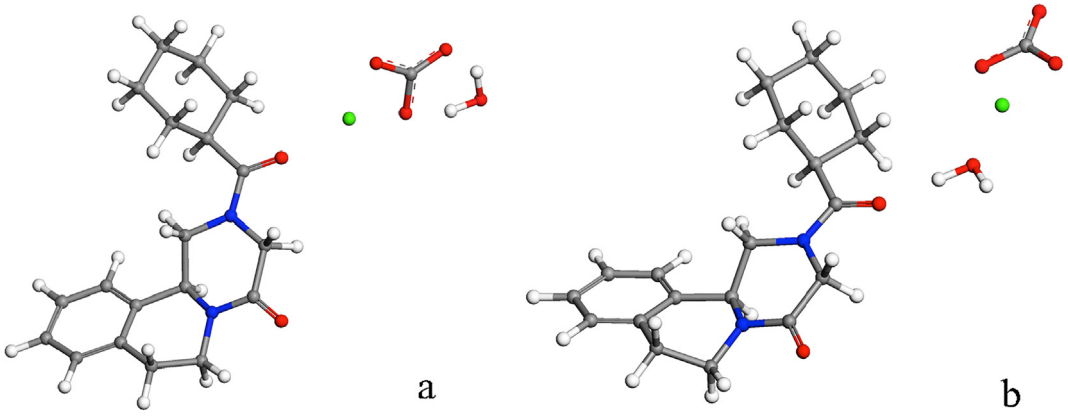

Fig. 14. Models of PZQCCw1 (a), and PZQCCw2 (b) complexes optimized with Compass. The C, Ca, H, N, and O atoms are in grey, green, white, blue, and red color. (For interpretation of the references to color in this figure legend, the reader is referred to the web version of this article.)

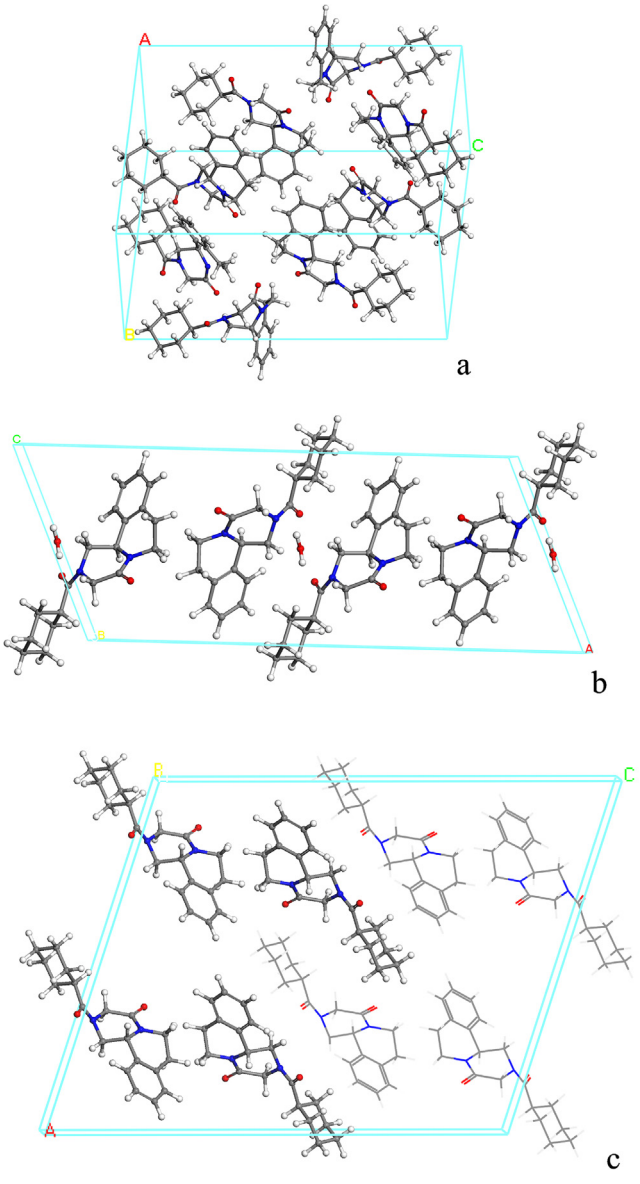

Fig. 15. Intermolecular interactions in the optimized crystal lattice of (RS)-PZQ (a), (R)-PZQ (b), the new RS polymorph (Form B) (The enantiomer S is highlighted with the atoms represented as balls) (c).

different molecular conformations, different intermolecular interactions and the presence of water molecules. In the (RS)-PZQ crystal both carbonyl groups are oriented to the same direction, conformation *syn*, whereas in the R-enantiomer hemihydrate crystal these carbonyl groups are oriented to opposite directions, conformation *anti*. In the crystal of the hemihydrate of the enantiomer (R)-PZQ (Fig. 15b), the crystallization water provides hydrogen bonds to connect the carbonyl groups.

In the crystal structure of the new RS polymorph (Form B), all PZQ molecules are in the anti conformation and the main intermolecular interactions are electrostatic between the carbonyl O atoms and the surrounding alkyl H atoms at d(CO···HC) = 2.6–2.9 Å. The unit cell is a racemic mixture with 4 molecules of each enantiomer per unit cell (Fig. 15c). However, the relative distribution of enantiomers is different from that of the pristine (RS)-PZQ. The enantiomers R are separate from the S ones forming clusters that form alternate slabs of each enantiomer in a tridimensional supercell structure, whereas in the initial pristine (RS)-PZQ the molecules are forming pairs of R and S enantiomers. The cohesion energy (−41.42 kcal/mol per PZQ molecule) of this new RS polymorph (Form B) is similar to the initial pristine (RS)-PZQ crystal form, −39.78 kcal/mol per PZQ molecule. This small energy difference can indicate a similar probability for nucleating both polymorphs.

The IUPAC definition of the term “racemic mixture” in the solid state refers to a heterogeneous mixture of two separate solid phases, while the term “racemate” refers to a homogeneous single phase [41]. Pseudoracemate is other possible solid structure that can be defined in chiral compounds. When one enantiomer has a greater affinity for molecules of its own kind than for those of the other enantiomer, both enantiomers crystallize in separate phases forming a racemic mixture. On the contrary, one enantiomer can have greater affinity for molecules of the opposite enantiomer than for its own kind and form a racemic compound. In both cases, the unit cell of the crystal lattice contains an equal number of molecules of each enantiomer and the product is a true addition compound. When there is little difference in the affinity between enantiomers of like or opposite configuration, both enantiomers exist in a disordered manner in the crystal forming a racemic solid solution or pseudoracemate [41]. In this work, one additional difference exists, that is, pure enantiomers form a different crystal polymorph with respect to the racemate. Liu et al. [11] studied several mixtures of PZQ enantiomers finding different melting points and concluded that the direct transformation between racemic mixture and racemic compound was not possible. However, in this work we conclude the opposite way. In the experimental crystallographic CIF file of (RS)-PZQ crystal (TELCEU, CCDC-896767), four PZQ molecules (two enantiomers pairs) per unit cell are disordered in the atomic positions of the aromatic-heterocyclic moiety of the molecule [15]. This mobility of the molecules could favor the easy polymorphic change in this system. Zanolla et al. [20] obtained the new polymorph just by milling physically without dissolution-recrystallization process. The conformer *anti* is less polar than the *syn* one, and the *anti* one is more stable than *syn* without polar interactions [37]. The mechanical energy during the grinding process can provoke a disorder in the molecules and a conformational change obtaining the most stable conformer. However, the ordering of this system did not produce a racemate, like in the initial (RS)-PZQ, but a pseudoracemate or racemic mixture where each enantiomer of the same sign is clustered.

After the dissolution of PZQ and treatment with GCC, both enantiomers precipitate forming a mixture of a solid solution of PZQ enantiomers (pseudoracemate) showing a melting point at 134–137 °C and some crystals of PZQ with a melting point at 111–113 °C. Previous authors [11] found a melting point at 111 °C of the crystal form of the enantiomer (-)-(R)-PZQ and a melting point at 134–138 °C for a 50:50 mixture of enantiomers of PZQ, indicating that this mixture was a racemate and not a conglomerate of enantiomers. In our work, the hemihydrate crystals of the separate enantiomers have the same melting point that the Form B. This can confuse in the interpretation of the polymorphic changes. In our experiments, the interaction of the calcium carbonate provokes the alteration of the pristine (RS)-PZQ that is not observed with a more inert excipient like colloidal silica. However, the presence of water is also critical for this alteration to form crystals that melt at 111–112 °C. This water content cannot be detected in our thermal analysis because it is embedded in the hemihydrate crystals. Therefore, we can conclude that these formed crystals, with melting point at 111–112 °C, could be assigned to the polymorph of hemihydrate of (R) and (S)-PZQ in separate crystals, instead of the anhydrous RS polymorph, Form B, reported by Zanolla et al. [20]. Nevertheless, DSC analysis did not distinguish the presence between the enantiomers and Form B crystals, or the formation of both polymorphs.

Besides, the DSC experiments of this work can identify clearly the melting points of the monoenantiomeric crystal or the Form B [20] (110–112 °C) and the pure racemic crystals (142–144 °C). However, new solid forms have been detected with intermediate melting points (134–138 °C), which cannot be clearly assigned. This happened only with the presence of calcium carbonate and can be produced also with and without the presence of water, indicating that could correspond to anhydrous forms. The solid phase with a melting point at 134 °C could

be assigned to another pseudoracemate or (RS)-racemate with defects and we cannot know its crystal structure. On the other hand, the solid phase with melting point at 138 °C could be another solid solution of enantiomers. Any of these phases could correspond tentatively to the initial racemate where the presence of defects or disordered PZQ could decrease its melting point. However, the phase with melting point at 134 °C is metastable and is transformed slowly to the phase whose melting point is 138 °C.

6. Conclusions

Our experiments conclude that the GCC used as excipient of the PZQ through the formation of a solid dispersion affected the crystal structure of the PZQ and modified the pristine PZQ solid state. This effect was enhanced with the presence of residual water molecules from the solvent. A crystal form change occurred along with conformational changes in the molecules. These modifications of the crystal forms could correspond either to monoenantiomeric forms or to the (RS)-Form B (melting point at 112 °C) and other phases (melting point at 134–138 °C) that could be tentatively assigned to a disordered pseudoracemate solid phases. These crystallographic changes were not observed using colloidal silica as solid excipient.

This phenomenon is due to the interaction of calcium carbonate with the carbonyl groups of PZQ, which are in the *syn* conformation. The presence of water is critical in the formation of the crystals with melting point at 111–112 °C. Probably the solvation water of Ca^{2+} cation forms hydrogen bonds with the carbonyl group joined to the cyclohexyl group. The PZQ molecule can adopt an *anti* conformation, which is energetically more stable than the syn one, like in the enantiomeric crystal. Then, the hydrated cyclohexyl-carbonyl group can interact with another PZQ molecule forming the hemihydrate enantiomer crystal (either the same enantiomer or a pseudoracemate crystal, if it is the other enantiomer) in a solid solution of mixed enantiomers.

Computational modeling, with classical FF and at quantum mechanical level, has been a useful tool for understanding the molecular interactions in the crystal structures and the effect of GCC on PZQ and the PZQ conformational changes in the crystal structures experimentally observed.

Acknowledgments

Authors are thankful to the regional Andalusian projects (RNM363 and RNM1897) and national MINECO project (FIS2016-77692-C2-2-P and CGL2016-80833-R) for financial support and to the Supercomputational Center of Universidad de Granada and CSIC for computing facilities.

References

[1] L. Chitsulo, D. Engels, A. Montresor, L. Savioli, The global status of schistosomiasis and its control, Acta Trop. 7 (2000) 41–51.
[2] P. Steinmann, J. Keiser, R. Bos, M. Tanner, J. Utzinger, Schistosomiasis and water resources development: systematic review, meta-analysis, and estimates of people at risk, Lancet Infect. Dis. 6 (2006) 411–425.
[3] R. Trastullo, L.S. Dolci, N. Passerini, B. Albertini, Development of flexible and dispersible oral formulations containing praziquantel for potential schistosomiasis treatment of pre-school age children, Int. J. Pharm. 495 (2015) 536–550.
[4] WHO, WHO Schistosomiasis, World Health Organization, http://www.who.int/es/news-room/fact-sheets/detail/schistosomiasis, 2018 (accessed 29 June 2018).
[5] D. Cioli, L. Pica-Mattoccia, S. Archer, Antischistomal drugs: past, present…and future? Pharmacol. Ther. 68 (1995) 35–85.
[6] D. Cioli, L. Pica-Mattoccia, Praziquantel, Parasitol. Res. 90 (2003) 3–9.
[7] EP 7.0. European Pharmacopoeia Seventh Edition. Directorate for the Quality of Medicines of the Council of Europe, Strasbourg, France, 2011.
[8] USP 36-NF31. United States Pharmacopoeia 36 and National Formulary 31. US Pharmacopoeial Convention, Rockville, MD USA, 2013.
[9] P. Andrews, Praziquantel: mechanisms of anti-schistosomal activity, Pharmacol. Ther. 29 (1985) 129–156.
[10] R. Pax, J.L. Bennett, R. Fetterer, A benzodiazepine derivative and praziquantel: effects on musculature of Schistosoma mansoni and Schistosoma japonicum, Naanyn-Schmiedeberg's Arch. Pharmacol. 304 (1978) 309–315.
[11] Y. Liu, X. Wang, J.K. Wang, C.B. Ching, Structural characterization and enantioseparation of the chiral compound praziquantel, J. Pharm. Sci. 93 (2004) 3039–3046.
[12] B.G. Lim, R.B.H. Tan, S.C. Ng, C.B. Ching, Solubility phase-diagram of praziquantel enantiomeric system, Chirality 7 (1995) 74–81.
[13] S.K. El-Arini, D. Giron, H. Leuenberg, Solubility properties of racemic praziquantel and its enantiomers, Pharm. Dev. Techn. 3 (1998) 557–564.
[14] Y. Liu, X. Wang, J.K. Wang, C.B. Ching, Investigation of the phase diagrams of chiral praziquantel, Chirality 18 (2006) 259–264.
[15] J.C. Espinosa-Lara, D. Guzmán-Villanueva, J.I. Arenas-García, D. Herrera-Ruiz, J. Rivera-Islas, P. Román-Bravo, H. Morales-Rojas, H. Höpfl, Cocrystals of active pharmaceuticals ingredients-praziquantel in combination with oxalic, malonic, succinic, maleic, fumaric, glutaric, adipic and pimelic acids, Cryst. Growth. Des. 13 (2013) 169–185.
[16] M. Lindenberg, S. Kopp, J.B. Dressman, Classification of orally administered drugs on the World Health Organization Model list of essential medicines according to the biopharmaceutics classification system, Eur. J. Pharm. Biopharm. 58 (2004) 265–278.
[17] D. González-Esquivel, J. Rivera, N. Castro, L. Yepez-Mulia, J.C. Helgi, In vitro characterization of some biopharmaceutical properties of praziquantel, Int. J. Pharm. 295 (2005) 93–99.
[18] N. Passerini, B. Albertini, B. Perissutti, L. Rodriguez, Evaluation of melt granulation and ultrasonic spray congealing as techniques to enhance the dissolution of praziquantel, Int. J. Pharm. 318 (2006) 92–102.
[19] A. Borrego-Sánchez, E. Carazo, C. Aguzzi, C. Viseras, C.I. Sainz-Díaz, Biopharmaceutical improvement of praziquantel by interaction with montmorillonite and sepiolite, Appl. Clay. Sci. 160 (2018) 173–179.
[20] D. Zanolla, B. Perissutti, N. Passerini, M.R. Chierotti, D. Hasa, D. Voinovich, L. Gigli, N. Demitri, S. Geremia, J. Keiser, P.C. Vioglio, B. Albertini, A new soluble and bioactive polymorph of praziquantel, Eur. J. Pharm. Biopharm. 127 (2018) 19–28.
[21] R.C. Rowe, P.J. Sheskey, P.J. Weller, Handbook of Pharmaceutical Excipients, sixth ed., Pharmaceutical Press, London, 2009.
[22] J.D. Martín-Ramos, XPowder software, http://www.xpowder.com, 2005 (accessed 29 June 2018).
[23] H. Sun, COMPASS: an ab initio force-field optimized for condensed-phase applications-overview with details on alkane and benzene compounds, J. Phys. Chem. B 102 (1998) 7338–7364.
[24] Accelrys Materials Studio, version v 6.0. Accelrys Inc., San Diego, USA, 2012.
[25] A. Borrego-Sánchez, C. Viseras, C. Aguzzi, C.I. Sainz-Díaz, Molecular and crystal structure of praziquantel. Spectroscopic properties and crystal polymorphism, Eur. J. Pharm. Sci. 92 (2016) 266–275.
[26] J.M. Soler, E. Artacho, J.D. Gale, A. García, J. Junquera, P. Ordejón, D. Sánchez-Portal, The Siesta method for ab initio order-N materials simulation, J. Phys. Condens. Matter. 14 (2002) 2745–2779.
[27] J.P. Perdew, K. Burke, M. Ernzerhof, Generalized gradient approximation made simple, Phys. Rev. Lett. 77 (1996) 3865–3868.
[28] N. Troullier, J.L. Martins, Efficient pseudopotentials for plane-wave calculations, Phys. Rev. B 43 (1991) 1993–2006.
[29] C.I. Sainz-Díaz, E. Escamilla-Roa, A. Hernández-Laguna, Quantum mechanical calculations of trans-vacant and cis-vacant polymorphism in dioctahedral 2:1 phyllosilicates, Am. Miner. 90 (2005) 1827–1834.
[30] R. Martos-Villa, M. Francisco-Márquez, M.P. Mata, C.I. Sainz-Díaz, Crystal structure, stability and spectroscopic properties of methane and CO_2 hydrates, J. Mol. Graph. Model. 44 (2013) 253–265.
[31] H.I. El-Subbagh, A.A. Al-Badr, Praziquantel, in: Florey (Ed.), Analytical Profiles of Drug Substances and Excipients, Academic Press Inc., New York, 1998, pp. 463–500.
[32] P. De la Torre, S. Torrado, S. Torrado, Preparation, dissolution and characterization of praziquantel solid dispersions, Chem. Pharm. Bull. 47 (1999) 1629–1633.
[33] M.V. Chaud, A.C. Lima, M.M.D.C. Vila, M.O. Paganelli, F.C. Paula, L.N. Pedreiro, M.P.D. Gremião, Development and evaluation of praziquantel solid dispersions in sodium starch glycolate, Trop. J. Pharm. Res. 12 (2013) 163–168.
[34] S.G. Rodrigues, I.S. Chaves, N.F.S. Melo, M.B. De Jesus, L.F. Fraceto, S.A. Fernandes, E. De Paula, M.P. De Freitas, L.M.A. Pinto, Computational analysis and physico-chemical characterization of an inclusion compound between praziquantel and methyl-β-cyclodextrin for use as an alternative in the treatment of schistosomiasis, J. Incl. Phenom. Macrocycl. Chem. 70 (2010) 19–28.
[35] F.B. Reig, J.V. Gimeno-Adelantado, M.C.M. Moya-Moreno, FTIR quantitative analysis of calcium carbonate (calcite) and silica (quartz) mixtures using the constant ratio method. Application to geological samples, Talanta 58 (2002) 811–821.
[36] N.V. Vagenas, A. Gatsouli, C.G. Kontoyannis, Quantitative analysis of synthetic calcium carbonate polymorphs using FT-IR spectroscopy, Talanta 59 (2003) 831–836.
[37] A. Borrego-Sánchez, A. Hernández-Laguna, C.I. Sainz-Díaz, Molecular modeling and infrared and Raman spectroscopy of the crystal structure of the chiral anti-parasitic drug praziquantel, J. Mol. Model. 23 (2017) 106.
[38] H.G.M. Edwards, S.E.J. Villar, J. Jehlicka, T. Munshi, FT–Raman spectroscopic study of calcium-rich and magnesium-rich carbonate minerals, Spectrochim. Acta A

61 (2005) 2273–2280.
[39] S.M. De Paula, M.F.G. Huila, K. Araki, H.E. Toma, Confocal Raman and electronic microscopy studies on the topotactic conversion of calcium carbonate from Pomacea lineate shells into hydroxyapatite bioceramic materials in phosphate media, Micron 41 (2010) 983–989.
[40] G.P.S. Smith, K.C. Gordon, S.E. Holroyd, Raman spectroscopic quantification of calcium carbonate in spiked milk powder samples, Vib. Spectrosc. 67 (2013) 87–91.
[41] A. Mitchell, Racemic drugs: racemic mixture, racemic compound, or pseudoracemate? J. Pharm. Pharm. Sci. 1 (1998) 8–12.